From Point Defects in Graphene to Two-Dimensional Amorphous Carbon

J. Kotakoski,[1,*] A. V. Krasheninnikov,[1,2] U. Kaiser,[3] and J. C. Meyer[3,†]

[1]*Department of Physics, University of Helsinki, Post Office Box 43, 00014 Helsinki, Finland*
[2]*Department of Applied Physics, Aalto University, Post Office Box 1100, 00076 Aalto, Finland*
[3]*Central Facility for Electron Microscopy, Group of Electron Microscopy of Materials Science, University of Ulm, 89081 Ulm, Germany*

(Received 8 October 2010; published 9 March 2011)

While crystalline two-dimensional materials have become an experimental reality during the past few years, an amorphous 2D material has not been reported before. Here, using electron irradiation we create an sp^2-hybridized one-atom-thick flat carbon membrane with a *random* arrangement of polygons, including four-membered carbon rings. We show how the transformation occurs step by step by nucleation and growth of low-energy multivacancy structures constructed of rotated hexagons and other polygons. Our observations, along with first-principles calculations, provide new insights to the bonding behavior of carbon and dynamics of defects in graphene. The created domains possess a band gap, which may open new possibilities for engineering graphene-based electronic devices.

DOI: 10.1103/PhysRevLett.106.105505 PACS numbers: 81.05.ue, 68.37.Og, 64.70.Nd, 71.15.Mb

Hexagonal rings serve as the building blocks for the growing number of sp^2–bonded low-dimensional carbon structures such as graphene [1,2] and carbon nanotubes [3]. Nonhexagonal rings usually lead to the development of nonzero curvature, e.g., in fullerenes [4] and carbon nanohorns [5], where the arrangement of other polygons can be geometrically deduced via the isolated pentagon rule (IPR) [4,6] and Euler's theorem [7]. Aberration-corrected high-resolution transmission electron microscopy (AC-HRTEM) has recently allowed atomic-resolution imaging of regular carbon nanostructures and identification of defects in these materials [8–12]. Point defects, mostly vacancies, are naturally created by the energetic electrons of a TEM. However, the possibility for selectively creating topological defects representing agglomerations of non-hexagonal rings could be more desirable in the context of carbon-based electronics. [13–15]

In fact, despite the recent advances, the precise microscopic picture of the response of graphene to electron irradiation remains incomplete. Earlier experiments on curved carbon nanosystems [16,17] have shown that they avoid under-coordinated atoms under irradiation at high temperatures via vacancy migration and coalescence. Recent experiments on graphene [12] reported only the development of holes. Theoretical studies have also predicted the appearance of small holes or formation of haeckelitelike configurations [18] or dislocations [19].

In this Letter, we report the transformation of graphene into a two-dimensional random arrangement of polygons due to continuous exposure to the electron beam with an energy just above the knock-on threshold. By carefully choosing the electron energy, we selectively enhance and suppress the underlying mechanisms of defect production. A combination of experiments and density-functional theory (DFT) calculations allows us to show that the transformation is driven by two simple mechanisms: atom ejection and bond rotation. The created defects tend to have a low formation energy and exhibit an electronic band gap. We also discover other unexpected configurations, such as stable carbon tetragons [20] which appear upon linear arrangement of divacancies.

Our graphene membranes were prepared by micromechanical cleavage and transfer to TEM grids [21]. Aberration-corrected HRTEM imaging was carried out in an FEI Titan 80–300, equipped with an objective-side image corrector. The microscope was operated at 80 and 100 keV for HRTEM imaging, and at 300 keV for irradiation. The extraction voltage of the field emission source was set to a reduced value of 2 kV in order to reduce the energy spread. For both 80 and 100 keV imaging, the spherical aberration was set to 20 μm and images were obtained at Scherzer defocus (ca. -9 nm). At these conditions, dark contrast can be directly interpreted in terms of the atomic structure.

The DFT calculations were carried out with the VASP simulation package [22,23] using projector augmented wave potentials [24] to describe core electrons, and the generalized gradient approximation [25] for exchange and correlation. Kinetic energy cutoff for the plane waves was 500 eV, and all structures were relaxed until atomic forces were below 0.01 eV/Å. The initial structure consisted of 200 C atoms, and Brillouin zone sampling scheme of Monkhorts-Pack [26] with up to $9 \times 9 \times 1$ mesh was used to generate the k points. Barrier calculations were carried out using the nudged elastic band method as implemented in VASP [27].

We started our experiments by monitoring *in situ* the behavior of graphene under a continuous exposure to electron irradiation using AC-HRTEM imaging with an electron energy of 100 keV, i.e., just above the threshold for knock-on damage (T_d) in sp^2-bonded carbon structures

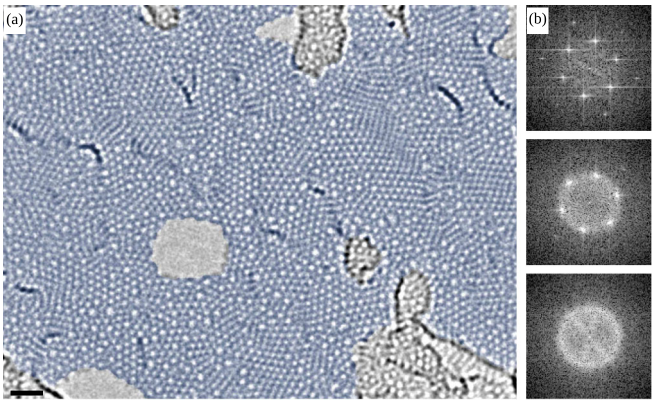

FIG. 1 (color online). (a) Amorphous two-dimensional sp^2-bonded carbon membrane created by a high-dose exposure of graphene to 100 keV electron irradiation in an HRTEM. The blue colored area is a single-layer carbon structure. Scale bar is 1 nm. (b) Fourier transforms (power spectra) from HRTEM images of the initial graphene configuration (top), an intermediate configuration (center), and of the amorphous 2D carbon (bottom).

[28,29]. Figure 1(a) shows a graphene structure after an electron dose of $\sim 1 \times 10^{10}$ e^-/nm^2. Contrary to the expectations, the structure does not predominantly consist of holes or collapse into a 3D object. Instead, it has remained as a coherent single-layer membrane composed of a random patch of polygons. Holes have also formed, but only on a small fraction of the area. The Fourier transform of the image shows that the resulting structure is completely amorphous [Fig. 1(b)].

In order to understand the mechanisms behind the transformation, we separated them by varying the electron beam energy. To observe how a defected graphene sheet reacts to an electron beam when atomic ejections are prohibited by a low enough electron energy, we created initial damage in a graphene sheet by brief 300 keV irradiation, and then studied the generated structures at 80 keV. Now only under-coordinated atoms can be ejected (T_d for a sp^2—bonded C is about 18–20 eV [28,29], whereas DFT calculations predict a T_d of $\sim$14 eV for a two-coordinated C). However, bond reorganization is possible, as activation energies for bond rotations in sp^2-bonded carbon structures are in the range of 4–10 eV [30,31], depending on the local atomic configuration. Correspondingly, in pristine graphene, bond rotations are occasionally observed under 80 keV irradiation [9] [Figs. 2(a) and 2(b)], resulting in the formation of the Stone-Wales defect [32]. In all observed cases continued exposure reversed this transition in pristine graphene. However, defect structures, e.g., divacancies, can convert between different configurations [Figs. 2(d)–2(f)] via bond rotations. According to our DFT simulations, the barriers for bond rotations in these structures are 5–6 eV, which excludes thermally activated migration in our room temperature experiments.

In Figs. 3(a)–3(d) we present evolution of a more complex defect structure. The defects created by an electron beam are predominantly monovacancies, which quickly

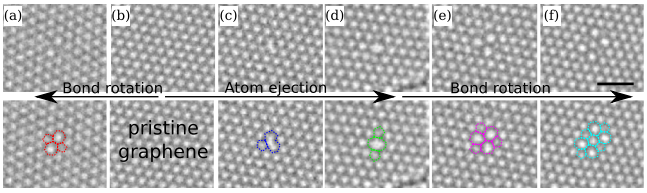

FIG. 2 (color online). Elementary defects and frequently observed defect transformations under irradiation. Atomic bonds are superimposed on the defected areas in the bottom row. Creation of the defects can be explained by atom ejection and reorganization of bonds via bond rotation. (a) Stone-Wales defect, (b) defect-free graphene, (c) V_1(5-9) single vacancy, (d) V_2(5-8-5) divacancy, (e) V_2(555-777) divacancy, (f) V_2(5555-6-7777) divacancy. Scale bar is 1 nm.

convert to divacancies due to a higher probability for under-coordinated atoms to be ejected, as noted above. Here [Fig. 3(a)], a brief exposure to a 300 keV beam (dose $\sim 10^7$ e^-/nm^2) has created an isolated V_2(555-777) and a defect with 4 missing carbon atoms (two connected divacancies). During the image sequence, the 80 keV electron beam causes the structure to reorganize via bond rotations. The V_2(555-777) turns first into a V_2(5-8-5) [Fig. 3(b)] and then a dislocation dipole [Fig. 3(c)], before forming a defect composed of clustered divacancies [Fig. 3(d)]. Figures 3(a)–3(d) also present two frequently observed linear arrangements of divacancies.

Because atom ejection occurs at random positions, vacancies initially appear randomly in the area exposed to the electron beam. However, during lower-energy exposure (e.g., 80 keV), these defects travel via a rebonding mechanism, which is illustrated in Fig. 3(e). Each migration step is initiated by a single electron impact

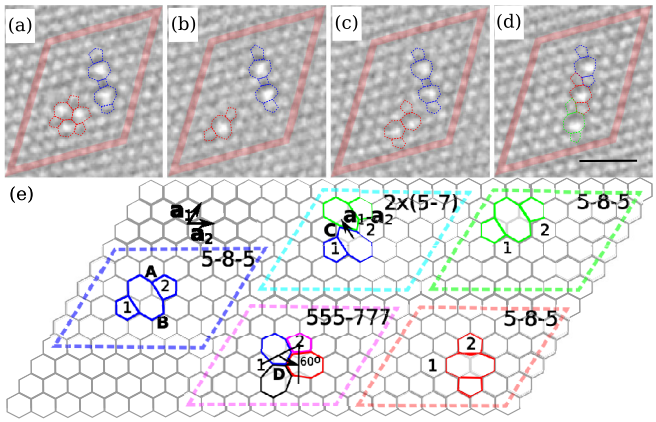

FIG. 3 (color online). (a)–(d) Electron beam driven divacancy migration observed at 80 keV. In (e), the changes in the bond configuration required for allowing the migration of a divacancy are shown. Transformation V_2(5-8-5) $\rightarrow 2 \times$ (5-7) is initiated by rotating bond A, and V_2(5-8-5) $\rightarrow V_2$(555-777) by rotating bond B. Rotating bonds C and D will lead to the final V_2(5-8-5) structures. In the first case the defect has moved by $\mathbf{a}_1$-$\mathbf{a}_2$, and in the second case it has rotated by 60° around pentagon 2. The original TEM images without overlays for panels (a)–(d) are presented in Ref. [33].

from which the atom obtains energy slightly below T_d. In other words, electron irradiation provides the activation energy to drive the system from a local energy minimum into another one, in our case predominantly via (reversible) bond rotations [Figs. 2(d)–2(f), Figs. 3(a)–3(d)]. This can be clearly seen in video S4 in Ref. [33] [partially shown in Figs. 3(a)–3(d)], where the configuration changes frequently until it arrives in the more stable configuration composed of three aligned double-vacancies.

Individual transitions can also lead to higher energy structures. For example, the intermediate states for the divacancy migration (dislocation dipole [Fig. 3(c)] and V_2(555-777) [Fig. 3(a)]) have formation energies E_f which differ from that of the V_2(5-8-5) by $\sim +3.72$ eV and ~ -0.66 eV, respectively. Aligning divacancies along the zigzag direction of the lattice [Fig. 3(d)], $\sim$1.32 eV of energy is gained per a divacancy pair, as compared to isolated divacancies. When the alignment appears along the armchair direction [Figs. 3(a)–3(c)], the energy gain is 2.01 eV. In this case, a tetragon is formed where the two pentagons of the adjacent divacancies would overlap. HRTEM simulation of the DFT-optimized structure of the defect is in excellent agreement with the experimental image [33]. Note that sp^2-bonded carbon tetragons in molecules, as in cyclobutadiene, can be stabilized only at low temperatures and when the molecules are embedded into a matrix [20]. In our case they are stabilized by the surrounding graphene lattice, as theoretically predicted for nanotubes [34].

Under 100 keV irradiation, atom ejection occurs at a very slow rate, so that changes in the atomic network are sufficiently slow to be precisely resolved. Therefore, the reconstruction of vacancy defects via bond rotations can be monitored immediately after a vacancy is generated. An example is presented in Fig. 4. The initial configuration [Fig. 4(a)] consists of three divacancies in the armchair orientation (formed prior to recording the first image). In the recorded images, the structure loses atoms until 24 atoms are missing. Several remarkable configurational changes are found in this image sequence. Figures 4(a)–4(c) show a collapse of linearly clustered defects into an apparently less defective structure with a dislocation dipole. This corresponds to the prediction of Jeong *et al.* [19] that the dislocation dipole is favored over a large multivacancy. However, this requires a linear arrangement of vacancies. Figures 4(a)–4(c) show the loss of four additional atoms. Two of them gave rise to an additional divacancy; the other two contributed to the separation of the dislocation cores (the rotated hexagon, clustered with a Stone-Wales defect, constitutes a dislocation core). During continued irradiation, we see the formation of a cluster of rotated hexagons surrounded by a chain of alternating pentagons and heptagons [Figs. 4(e)–4(h)]. Such configurations, rotated by 30° with respect to the original lattice and matched by pentagons and heptagons to the zigzag lattice direction, appear to be the preferred way to incorporate missing atoms in the graphene structure. Because of the matching numbers of

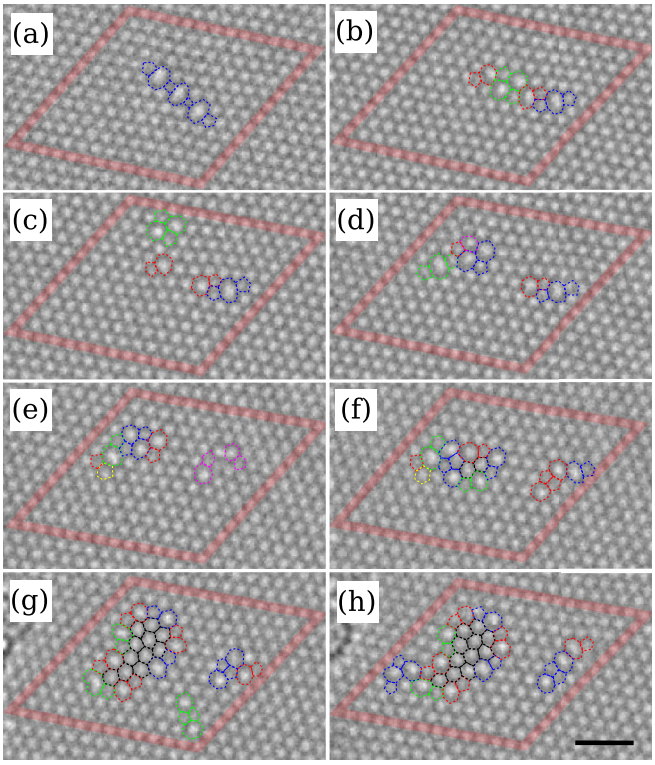

FIG. 4 (color online). Formation of rotated-hexagon kernels in multivacancy structures under a 100 keV electron beam. Scale bar is 1nm. The original TEM images without overlays are presented in Ref. [33].

pentagons and heptagons—and hence cancellation of negative and positive curvature—these structures remain flat.

To understand the driving force for the transformations, we calculated E_f for the simplest defect structures matching the observed trend of forming a rotated-hexagon kernel. The lowest-energy tetra-vacancy (four missing atoms) can be created by combining two V_2(5555-6-7777) divacancies, whereas the hexavacancy (six missing atom) requires three of these defects [Fig. 5(a)]. Remarkably, these configurations have the lowest E_f of any reported vacancy structures with equal number of missing atoms in graphene (E_f per missing atom multiplied by the number of missing

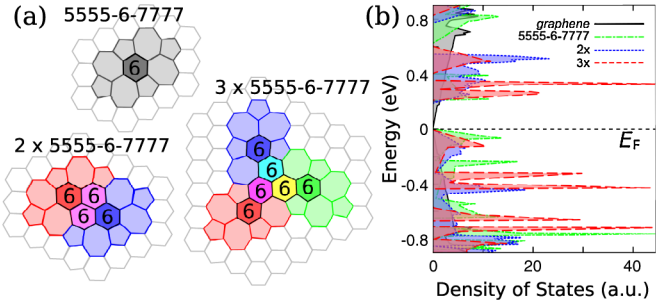

FIG. 5 (color online). dealized rotated-hexagon defects (a) formed from one, two, and three V_2(5555-6-7777) divacancy defects, as optimized with DFT calculations. Electronic density of states (b) for pristine graphene and the structures presented in panel (a).

atoms are $\sim 4 \times 3.14$ eV and $\sim 6 \times 2.50$ eV). A hole with six missing atoms has a formation energy of $\sim 6 \times 3.15$ eV, while for a dislocation and a haeckelitelike structure values of $\sim 6 \times 3.72$ eV and $\sim 6 \times 2.64$ eV have been reported [19], respectively. Evidently, the rotated-hexagon defects spawn the family of lowest-energy multivacancies in graphene. In contrast to what was recently shown for the zigzag-oriented divacancies [14], these structures open a band gap in graphene, as can be seen from the density of states [Fig. 5(b)]. The calculated band gap is in the order of 200 meV. This value is possibly underestimated within the used GGA approximation, and advanced DFT methods are likely to give a higher value [35].

To conclude, we have shown how an electron beam can be used to selectively suppress and enhance bond rotations and atom removal in graphene. We demonstrated that irradiation at electron energies just above the threshold for atom displacement turns graphene not into a ''perforated graphene'' but a two-dimensional coherent amorphous membrane composed of sp^2—hybridized carbon atoms. This membrane grows through nucleation and expansion of defects which result from electron beam–driven divacancy migration and agglomeration. These defect configurations predominantly consist of a 30° rotated kernel of hexagons surrounded by a chain of alternating pentagons and heptagons. These defects are the energetically favored way for the graphene lattice to accommodate missing atoms, and have a semiconducting nature. Since several of the presented examples of the two-dimensional sp^2-hybridized defect configurations violate the IPR, due to increased reactivity [6,36], they may be exploited for functionalization of graphene. We also showed unambiguous evidence for four-membered carbon rings in graphitic structures. Clearly, despite the large amount of research, the richness of carbon chemistry continues to provide surprises. More examples of the observed structures and videos of the complete TEM image series are presented in Ref. [33].

We acknowledge support by the German Research Foundation (DFG) and the German Ministry of Science, Research and the Arts (MWK) of the state Baden-Wuerttemberg within the SALVE (sub angstrom low voltage electron microscopy) project and by the Academy of Finland through several projects. We are grateful for the generous grants of computer time provided by CSC Finland.

*Corresponding author.
jani.kotakoski@iki.fi
†Present address: University of Vienna, Department of Physics, 1090 Wien, Austria.

[1] K. S. Novoselov, A. K. Geim, S. V. Morozov, D. Jiang, Y. Zhang, S. V. Dubonos, I. V. Grigorieva, and A. A. Firsov, Science **306**, 666 (2004).
[2] K. S. Novoselov, D. Jiang, F. Shedin, T. J. Booth, V. V. Khotkevich, S. V. Morozov, and A. K. Geim, Proc. Natl. Acad. Sci. U.S.A. **102**, 10 451 (2005).
[3] S. Iijima, Nature (London) **354**, 56 (1991).
[4] H. W. Kroto, Nature (London) **329**, 529 (1987).
[5] S. Iijima, M. Yudasaka, R. Yamada, S. Bandow, K. Suenaga, F. Kokai, and K. Takahashi, Chem. Phys. Lett. **309**, 165 (1999).
[6] T. G. Schmalz, W. A. Seitz, D. J. Klein, and G. E. Hite, J. Am. Chem. Soc. **110**, 1113 (1988).
[7] H. Terrones and A. L. Mackay, Carbon **30**, 1251 (1992).
[8] A. Hashimoto, K. Suenaga, A. Gloter, K. Urita, and S. Iijima, Nature (London) **430**, 870 (2004).
[9] J. C. Meyer, C. Kisielowski, R. Erni, M. D. Rossell, M. F. Crommie, and A. Zettl, Nano Lett. **8**, 3582 (2008).
[10] M. H. Gass, U. Bangert, A. L. Bleloch, P. Wang, R. R. Nair, and A. K. Geim, Nature Nanotech. **3**, 676 (2008).
[11] C. O. Girit *et al.*, Science **323**, 1705 (2009).
[12] J. H. Warner, M. H. Rummeli, L. Ge, T. Gemming, B. Montanari, N. M. Harrison, B. Buchner, and G. A. D. Briggs, Nature Nanotech. **4**, 500 (2009).
[13] A. H. Castro Neto, F. Guinea, N. M. R. Peres, K. S. Novoselov, and A. K. Geim, Rev. Mod. Phys. **81**, 109 (2009).
[14] J. Lahiri, Y. Lin, P. Bozkurt, I. I. Oleynik, and M. Batzill, Nature Nanotech. **5**, 326 (2010).
[15] O. V. Yazyev and S. G. Louie, Nature Mater. **9**, 806 (2010).
[16] L. Sun, F. Banhart, A. V. Krasheninnikov, J. A. Rodríguez-Manzo, M. Terrones, and P. M. Ajayan, Science **312**, 1199 (2006).
[17] L. Sun, A. V. Krasheninnikov, T. Ahlgren, K. Nordlund, and F. Banhart, Phys. Rev. Lett. **101**, 156101 (2008).
[18] H. Terrones, M. Terrones, E. Hernández, N. Grobert, J.-C. Charlier, and P. M. Ajayan, Phys. Rev. Lett. **84**, 1716 (2000).
[19] B. W. Jeong, J. Ihm, and G.-D. Lee, Phys. Rev. B **78**, 165403 (2008).
[20] Y.-M. Legrand, A. v. d. Lee, and M. Barboiu, Science **329**, 299 (2010).
[21] J. C. Meyer, C. O. Girit, M. F. Crommie, and A. Zettl, Appl. Phys. Lett. **92**, 123110 (2008).
[22] G. Kresse and J. Furthmüller, Comput. Mater. Sci. **6**, 15 (1996).
[23] G. Kresse and J. Furthmüller, Phys. Rev. B **54**, 11 169 (1996).
[24] P. E. Blöchl, Phys. Rev. B **50**, 17953 (1994).
[25] J. P. Perdew, K. Burke, and M. Ernzerhof, Phys. Rev. Lett. **77**, 3865 (1996).
[26] H. J. Monkhorst and J. D. Pack, Phys. Rev. B **13**, 5188 (1976).
[27] G. Henkelman, B. P. Uberuaga, and H. Jónsson, J. Chem. Phys. **113**, 9901 (2000).
[28] F. Banhart, Rep. Prog. Phys. **62**, 1181 (1999).
[29] B. W. Smith and D. E. Luzzi, J. Appl. Phys. **90**, 3509 (2001).
[30] C. P. Ewels, M. I. Heggie, and P. R. Briddon, Chem. Phys. Lett. **351**, 178 (2002).
[31] L. Li, S. Reich, and J. Robertson, Phys. Rev. B **72**, 184109 (2005).
[32] A. J. Stone and D. J. Wales, Chem. Phys. Lett. **128**, 501 (1986).
[33] See supplemental material at http://link.aps.org/supplemental/10.1103/PhysRevLett.106.105505.
[34] W. Orellana, Phys. Rev. B **80**, 075421 (2009).
[35] D. J. Appelhans, Z. Lin, and M. T. Lusk, Phys. Rev. B **82**, 073410 (2010).
[36] Y.-Z. Tan, S.-Y. Xie, R.-B. Huang, and L.-S. Zheng, Nature Chem. **1**, 450 (2009).